



Microstructure and crystallographic texture of *Charonia lampas lampas* shell

S. Ouhenia^{a,b,*}, D. Chateigner^a, M.A. Belkhir^b, E. Guilmeau^a

^a Laboratoire CRISMAT-ENSICAEN (CNRS UMR 6508), Université de Caen Basse-Normandie, 6 bd M. Juin, 14050 Caen, France

^b Laboratoire de physique, faculté des sciences exactes, Bejaia 06000, Algeria

ARTICLE INFO

Article history:

Received 10 April 2008

Received in revised form 13 May 2008

Accepted 14 May 2008

Available online 23 May 2008

Keywords:

Biomineralisation

Aragonite

Organic matrix

Texture

XRD

X-ray diffraction

Charonia

ABSTRACT

Charonia lampas lampas shell is studied using scanning electron microscopy and X-ray diffraction combined analysis of the preferred orientations and cell parameters. The *Charonia* shell is composed of three crossed lamellar layers of biogenic aragonite. The outer layer exhibits a (001) fibre texture, the intermediate crossed lamellar layer is radial with a split of its *c*-axis and single twin pattern of its *a*-axis, and the inner layer is comarginal with split *c*-axis and double twinning. A loss of texture strength is quantified from the inner layer outward. Unit-cell refinements evidence the intercrystalline organic influence on the aragonite unit-cell parameters anisotropic distortion and volume changes in the three layers. The simulation of the macroscopic elastic tensors of the mineral part of the three layers, from texture data, reveals an optimisation of the elastic coefficient to compression and shear in all directions of the shell as an overall.

© 2008 Elsevier Inc. All rights reserved.

1. Introduction

Biogenic crystals attract large attentions because of their superior properties on many aspects. While commonly involved in skeletal support or protection of cells and soft tissues, some biomineralized structures also have evolved to fulfil highly specific functions in demanding environments. For example, the iron oxide-based magnetosomes used to orient bacteria in the earth's magnetic field (Sakaguchi et al., 1993; Bazylinski, 1996), and the radula teeth used by chitons to scrape nutrients off rocks in the intertidal zone (Lowenstam, 1967). The process of biomineralisation is realised with a minimum consumption of energy and a precise control on the polymorphism and crystal morphology (Ouhenia et al., 2008) on a nanometre-scale by the use of organic macromolecules secreted by the organism according to its genetic programming.

The complete understanding of biomineral development processes is still subject to debates and strongly motivated by their potential utility in industrial and biomedical applications (Murphy and Mooney, 2002). A deeper understanding of the mineralisation process and the mimicking of complex structures produced by nature in laboratory may have a significant impact on many fields such as the development of new composite materials, drug delivery, bone replacement, device fabrication in microelectronics and optoelectronics. For instance, aragonitic biominerals, like nacre

layers from *Pinctada margaritifera*, are ideal biomedical implants, and thanks to their high aspect ratio, aragonite crystals can be used as reinforcements in composite materials (Sugawara and Kato, 2000).

Molluscan shells are fascinating examples of high performance organic/inorganic biocomposite materials. Although the organic components represent only about 1–5% the weight of the shell (Hare and Abelson, 1965; Cariolou and Morse, 1988), they provide nanoscale precision of control over shell fabrication and are responsible for the remarkable enhancement of the strength and elasticity of the material as compared to geological mineral. The toughness of red abalone nacre *Haliotis rufescens* is 3000 times higher than the value for pure aragonite (Currey, 1977; Jackson et al., 1990; Kamat et al., 2000), and toughening mechanisms deduced from the crack propagation behaviour in nacre are attributed to the structural relationship between the organic macromolecules and inorganic crystals (Chen et al., in press; Smith et al., 1999). Molluscan shells are mainly built of two polymorphs of calcium carbonate: calcite and aragonite. Most of the organic phase is located between crystallites (intercrystalline), but some organic molecules (intracrystalline) are also intercalated within the crystalline lattice. Recently, using very precise synchrotron measurements, Pokroy et al. (2004, 2006) have shown that the biogenic unit-cell is anisotropically distorted compared to the non-biogenic reference, a distortion attributed to the incorporated intracrystalline organic molecules.

In this work, the preferred crystallographic orientation of the aragonitic shell of the Gastropod *Charonia lampas lampas* is examined using X-ray texture and unit-cell combined analysis. Based on

* Corresponding author. Address: Laboratoire CRISMAT-ENSICAEN (CNRS UMR 6508), Université de Caen Basse-Normandie, 6 bd M. Juin, 14050 Caen, France.

E-mail address: salim.ouhenia@ensicaen.fr (S. Ouhenia).

the combination of quantitative texture formalism and Rietveld refinement, this approach allows to work on the real layers of the shell without necessity of powderisation, and provides the orientation distributions of the three layers of the shell, together with their unit-cell refinement. We examine the correspondence between textures and morphology (as seen by scanning electron microscopy) of the shell structures. The unit-cell anisotropic distortions are discussed in terms of intercrystalline and intracrystalline influences. Finally, the macroscopic elastic behaviour of the mineral parts of the layers is simulated and discussed.

2. Experimental

2.1. Materials

The Gastropod *C. lampas lampas* (Linnaeus 1758) is a large Mediterranean Sea and Eastern Atlantic carnivorous mollusc from the Ranellidae (tritons and trumpet shells) family (Beu, 1985, 1987), Tonnoidea superfamily, Caenogastropoda. This species is one of the 17 species protected by the Bern convention for the Mediterranean sea. We collected a 15 cm large shell from a deceased animal (Fig. 1a) from the coast of Bejaia, in the north east area of Algeria (North Africa). The inorganic part of the shell is only composed of aragonite (CaCO_3 , Pmcn space group). An SEM image at low magnification (Fig. 1b) of the *C. lampas lampas* fractured shell studied here shows three distinct layers which we will refer to outer, intermediate and inner layers from top to bottom, respectively.

In order to carry out X-ray diffraction analysis, we removed a piece of the shell (Fig. 1a) from the dorsum, as flat as possible (for technical reasons, the sample for texture analysis needs to

be close to planar, uneven surfaces giving rise to uncontrolled defocusing and absorption of the beam). This piece was centred on a (**G**,**N**,**M**) frame defined by the main shell directions identified using optical microscopy (Chateigner et al., 2000):

- The growth direction, **G**, perpendicular to the margin of the shell (Fig. 1) is the vertical axis of our pole figures.
- The plane tangent to the shell at the beam location, defined by the sample holder plane, has its normal, **N**, as the normal axis in the centre of the pole figures.
- The third axis, **M**, direction of the growth lines of the outer layer, is horizontal in the pole figures.

We first measured the exterior of the shell (the outer layer), then removed this layer with a diluted solution of HCl to analyse the intermediate layer, and repeated the same operation with the intermediate layer to measure the inner one in the same conditions.

2.2. Characterisation

We examined the shell microstructures of gold-sputtered fractured cross-sections using a Zeiss scanning electron microscope (SEM) with an accelerating voltage of 3 kV. X-ray diffraction measurements were carried out using a four-circle goniometer (Huber) mounted on a X-ray generator ($\text{CuK}\alpha$ radiation) equipped with a curved position-sensitive detector (CPS-120, Inel) covering an angle of 120° (2θ resolution 0.03°). A $5^\circ \times 5^\circ$ grid measurement in tilt and azimuthal angles was carried out to cover the whole pole figure, resulting in 936 diagrams measured for each layer. The use of a CPS detector accelerates considerably the data acquisition compared with point detectors, and gives access to other parameter refinements than texture, like cell parameters, atomic positions, etc. Pole figure data are normalised into distribution densities and expressed as multiple of a random distribution (mrd), which is equivalent to volume percentage per 1% area. A specimen with no preferred orientation has pole figures with constant values of 1 mrd. In order to deconvolute instrumental resolution function from sample data, we fitted this latter using a LaB_6 (SRM660b) standard from NIST. All data were analysed within the so-called “Combined Analysis” formalism (Chateigner, 2004) using the MAUD software (Lutterotti et al., 1999). The orientation distribution (OD) of crystallites was refined using the E-WIMV model (Lutterotti et al., 2004), and peaks extraction was carried out using the Le Bail approach. No residual stress could be visible in the layers.

3. Results and discussion

3.1. Scanning electron microscopy

The terminology of shell microstructures is usually based on the morphology of sub-units as observed in thin-sections with a petrographic microscope or with SEM. We describe the layer microstructures using the terminology of Carter and Clark (1985), but we emphasise that these definitions only represent a terminology (the names are convenient brief summaries of observed morphologies), not necessarily a statement of homology (Chateigner et al., 2000). We use ‘first-order’ and ‘second-order’ lamellae to describe increasingly fine microstructural elements with morphological distinction. For instance, simple crossed lamellar structure is composed of first-order lamellae (approximately $20\ \mu\text{m}$), each of which is composed of second-order lamellae ($0.1\ \mu\text{m}$ in thickness). If the plane of lamellae is parallel to the margin (the edge) of the shell (**M**), the structure is “comarginal”, but if it is perpendicular to it, then the structure is “radial”.

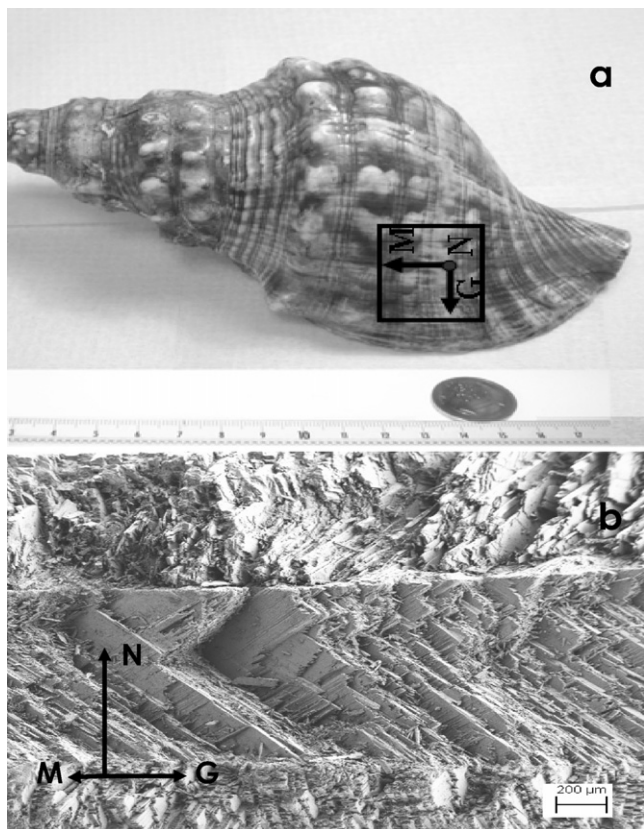


Fig. 1. (a) The *Charonia lampas lampas* shell studied in this work. (b) Cross-section SEM image of the fractured shell at the location indicated in (a). **G**, **M** and **N** indicate the Growth, Margin and Normal directions, respectively.

Fig. 1b shows the three layers of a broken section of the *Charonia* shell, with the outer layer on top of the figure, the plane of the fracture being inclined relative to (G,N). At this scale and using this inclination, all three layers exhibit crossed lamellae. The outer layer exhibits first-order lamellae parallel to the margin, like in comarginal crossed lamellar structures, but at several places the first-order lamellae deviate strongly from the M direction. The intermediate layer is composed of crossed lamellae closely parallel to the growth direction, like in a radial crossed lamellar structure. Finally, the inner layer shows lamellae parallel to M, like a comarginal layer. The total width of the sample at this location in the shell is around 1.5 mm, half of the thickness being dedicated to the intermediate layer, while the two other layers roughly occupy equivalently the remaining space.

Fig. 2a shows a zoom of the outer layer at a place where first-order lamellae are comarginal. Each first-order lamellae (approximately 15 μm thick) is composed of second-order lamellae (Fig. 2b) extending at least on several micrometres and with a thickness of about 0.1 μm . We also notice that there is only one orientation of the second-order lamellae in all adjacent first-order lamellae.

Fig. 3 shows details of the intermediate radial crossed lamellar layer. We can distinguish in this layer the existence of two types of lamellae from the orientation of their second-order lamellae. These latter make an acute angle (Fig. 3a) close to 90° between two adjacent first-order lamellae. A detailed view of the second-order

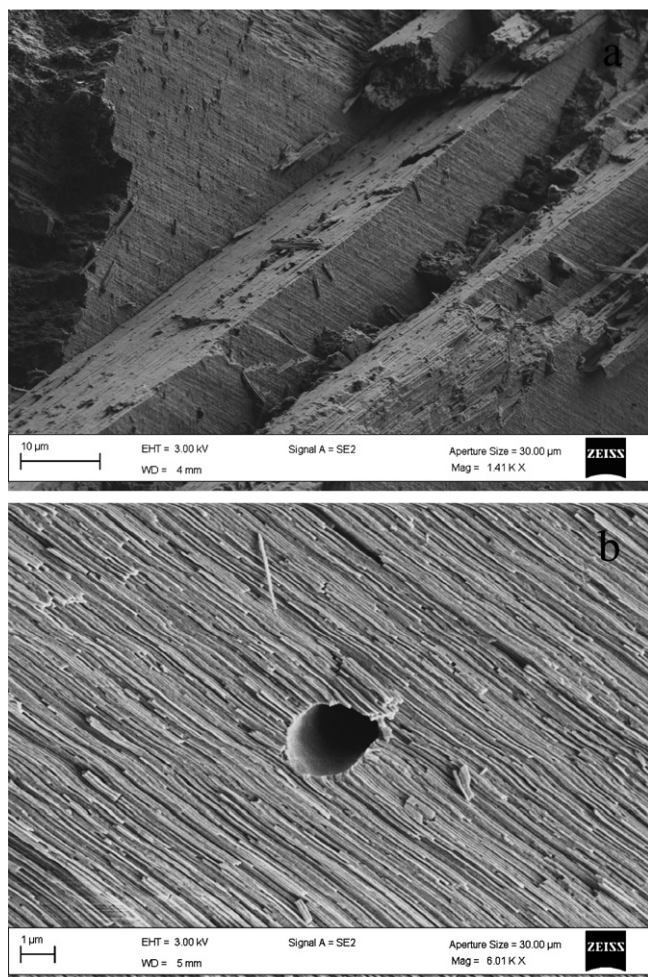


Fig. 2. SEM images of: (a) the outer comarginal lamellae (b) the second-order lamellae composing the first-order ones.

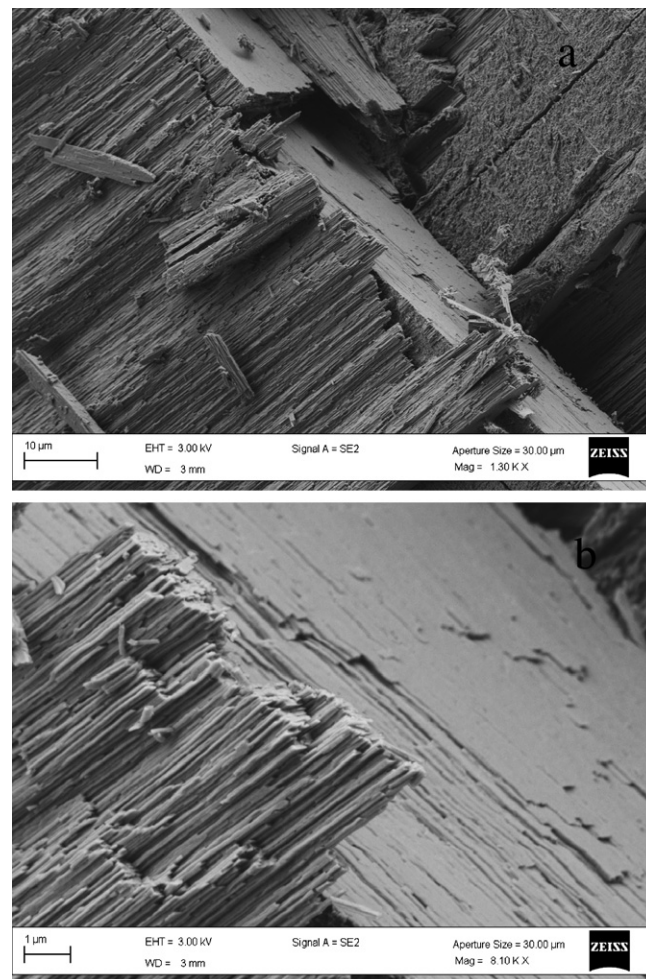


Fig. 3. SEM images of the first (a) and second (b) order lamellae of the intermediate radial crossed lamellar layer.

lamellae (Fig. 3b) indicates a thickness around 100 nm, a width extending to the whole width of the first-order lamellae (around 10 μm in this species), and a length out of the range of our image. If at some places the first-order lamellae from this layer appear at 90° from the ones of the outer layer, this is not the case everywhere (Fig. 1b) at the scale of 1 to several millimetres.

The detailed image of the inner comarginal crossed lamellar layer (Fig. 4) shows much more regularity in the lamellae stacking. The width of the first-order lamellae is around 15 μm , while the second-order lamellae are again around 100 nm thick. The angle between the long axis of second-order lamellae from two adjacent first-order lamellae is as for the intermediate layer around 90°. The first-order lamellae from this inner layer are perpendicular to the ones of the intermediate layer.

3.2. Texture analysis results

The combined analysis refinements operated on the three layers converge to reasonably good solutions with low reliability factors and goodness-of-fits (GoF) not above 3.05 (Table 1). The Rietveld reliability factors could seem large compared to the literature *R* factors on single diagrams. However, one should bear in mind that these factors depend on the number of data points. In our case this latter is large (nearly 1.8×10^6), since we analyse each 2θ diagram in the 28–85° range with a 0.03° equivalent step (1900 points/diagram) and 936 diagrams. The texture reliability factors are also low

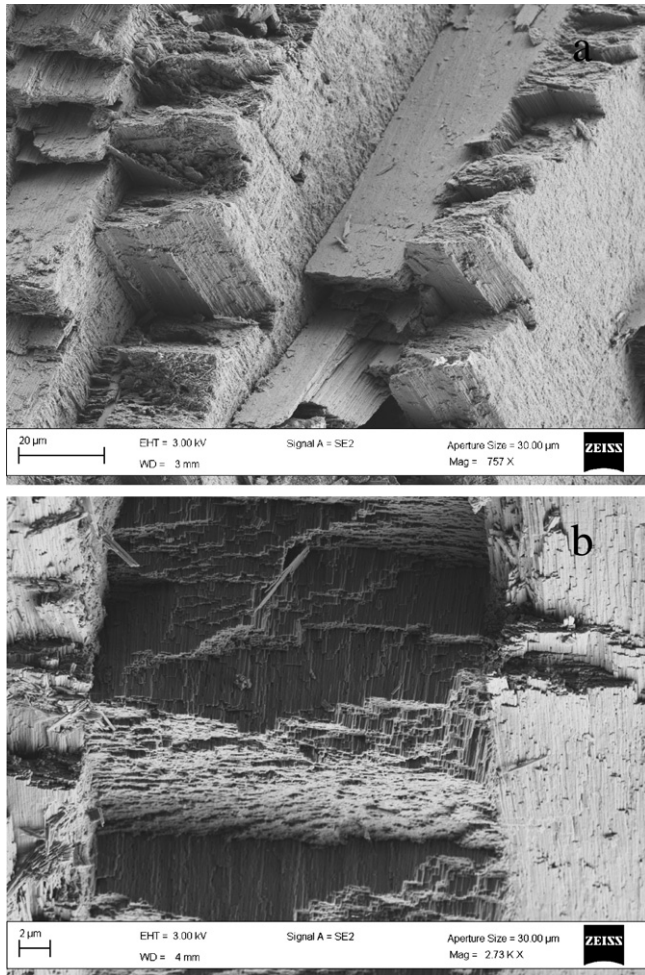


Fig. 4. SEM images of the first (a) and second (b) order lamellae of the inner comarginal crossed lamellar layer.

compared to similar texture strengths from the literature (Chateigner, 2005), as a sign of a good definition of the OD for the three layers. The inner layer, however, exhibits the largest factors and

GoF. This is mainly due to the relatively large scanning grid used in the measurement ($5^\circ \times 5^\circ$) compared to the sharpness of the poles, as will be seen later, and is not conditioning our results. A visualisation of the corresponding refinement quality can also be visible when looking at the reproduction of the experimental data using the combined analysis simulation (Fig. 5), on randomly selected diagrams. At few exceptions, the simulated lines correctly reproduce the experiments, again the inner layer being a bit less satisfactorily simulated, corresponding to its larger reliability factors. The experimental and recalculated diagrams (Fig. 5d) plotted in two dimensions clearly reveal the good fits obtained even in the inner layer. In such a plot the strong texture is clearly visible, with strong peak intensity variations with the (χ, ϕ) specimen orientation. For the three layers the OD minimum values are all zero (Table 1), indicating that all the crystallites are included in the described components of orientations. From the outer layer inward, the texture index F^2 is increasing. This indicates a largest crystalline organisation closer to the animal, which was already observed (Chateigner et al., 2000) for many species. The OD maximum value is lower for the intermediate than for the outer layer. This is due to the presence of two texture components in the former, and does not prompt for a weaker texture.

The outer crossed lamellar (OCL) layer of *C. lampas lampas* exhibits an overall texture strength of $F^2 = 42.6 \text{ mrd}^2$ (Table 1) which is among the moderate texture strengths of gastropod shells measured up to now (Chateigner et al., 2000). This is mainly due to the fibre character of the texture (Fig. 5a), as demonstrated by the homogeneous ring exhibited by the $\{200\}$, $\{020\}$ or $\{110\}$ pole figures. Indeed, the $\{002\}$ pole figure shows a strong maximum in its centre around 43 mrd , which is among high levels for crossed lamellar layers (Chateigner et al., 2000), but this strength is lowered on overall by the fibre character. This latter pole figure indicates that crystals are aligned with their *c*-axis perpendicular to the surface of the shell, with their mean orientation parallel to *N*, and a full width at half maximum of the distribution density (FWHD) around 20° . Such outer crossed lamellar (OCL) layers exhibiting a fibre texture are found in some other gastropods like *Viana regina*, *Conus leopardus* and *Cyclophorus woodianus*, the two former species exhibiting weaker orientations for this layer.

The intermediate radial crossed lamellar (RCL) layer texture shows a texture strength of 47 mrd^2 and a maximum of the

Table 1

Parameters resulting from the combined analysis of the outer, intermediate and inner layers of *Charonia lampas lampas*

Layer	Outer	Intermediate	Inner
<i>a</i> (Å)	4.98563(7)	4.97538(4)	4.9813(1)
<i>b</i> (Å)	8.0103(1)	7.98848(8)	7.9679(1)
<i>c</i> (Å)	5.74626(3)	5.74961(2)	5.76261(5)
$\Delta a/a$	0.0047	0.0026	0.0038
$\Delta b/b$	0.0053	0.0026	$-1\text{E}-05$
$\Delta c/c$	0.0004	0.001	0.0033
$\Delta V/V$	1.05%	0.62%	0.71%
OD maximum (mrd)	299	196	2816
OD minimum (mrd)	0	0	0
Texture index (mrd^2)	42.6	47	721
Texture reliability factors			
R_w (%)	14.3	11.2	32.5
R_B (%)	15.6	12.7	47.8
Rietveld reliability factors			
GoF (%)	1.72	1.72	3.05
R_w (%)	29.2	28	57.3
R_B (%)	22.9	21.7	47.2
R_{exp} (%)	22.2	21.3	32.8

Parentheses indicate standard deviations on the last digit. GoF, goodness-of-fit. We took as reference unit-cell for non-biogenic crystals: $a = 4.9623(3) \text{ \AA}$, $b = 7.968(1) \text{ \AA}$, $c = 5.7439(3) \text{ \AA}$ (ICDD Card No. 41-1475).

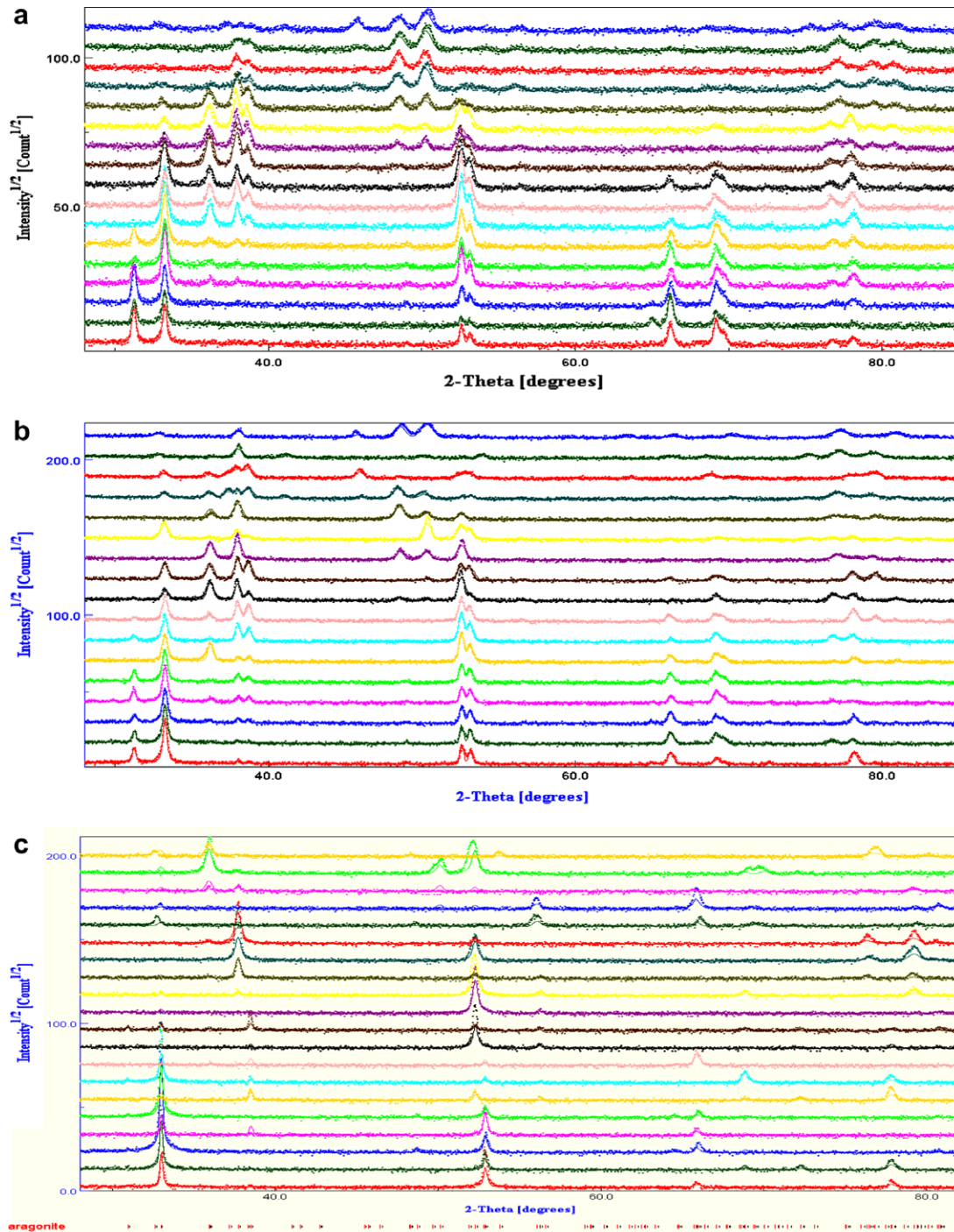


Fig. 5. Randomly selected diagrams showing the good reproducibility of the experimental (dots) patterns from the combined analysis refinement (lines) after the last refinement cycle for the (a) outer (b) intermediate and (c) inner layers. (d) Is a 2D plot of whole diagram datasets for the experimental (bottom) and recalculated (top) diagrams showing the reproducibility on all the diagrams (here for the intermediate RCL layer). Horizontal axis as 2θ , and vertical axis the diagram number from $(\chi, \phi) = (0,0)$ to $(60,355)$, refined diagrams at top, experiments at bottom.

{002} pole density around 26 mrd (Fig. 6b). The {002} pole figure evidences a split of the c -axis distribution around \mathbf{N} , with an opening angle of 20° between the two contributions, parallel to the (\mathbf{G}, \mathbf{N}) plane. Each of these two contributions has a FWHM of 10° . Furthermore, as seen on the {020} and {200} pole figures, the orientation of the a - and b -axes in the sample plane features a single twin distribution (Chateigner et al., 2000) with {110} twinning planes. The {110} pole figure indicates that the major 110 contri-

bution is for [110] directions parallel to \mathbf{M} . Such a texture was observed in the gastropods *Scutus antipodes* and *Patella (Scutellaster) tabularis*, for their crossed lamellar (CL) and inner radial crossed lamellar (IRCL) layers, with opening angles of 15° and 25° , and twinning occurring for 27% and 100%, respectively. The texture of the RCL layer of *C. lampas lampas* resembles more the one of the IRCL of *P. tabularis*, also from the comparison of their maxima of the {002} pole figures. Furthermore, *C. lampas lampas* exhibits its

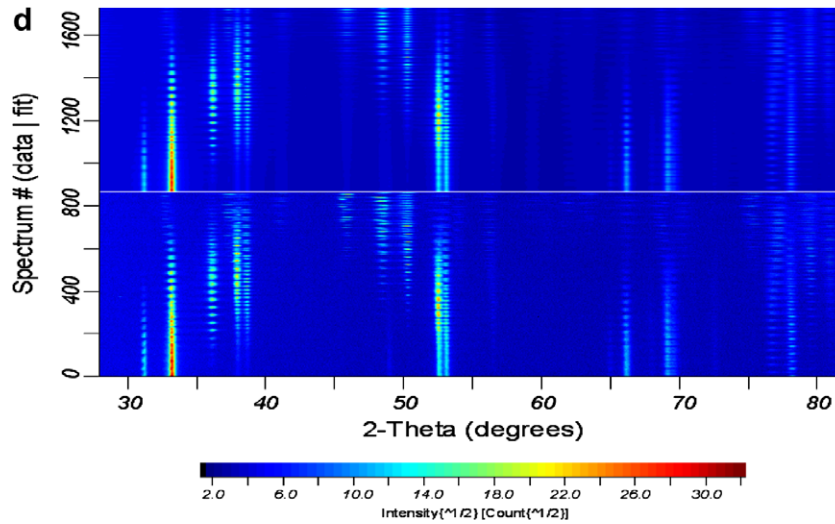


Fig. 5 (continued)

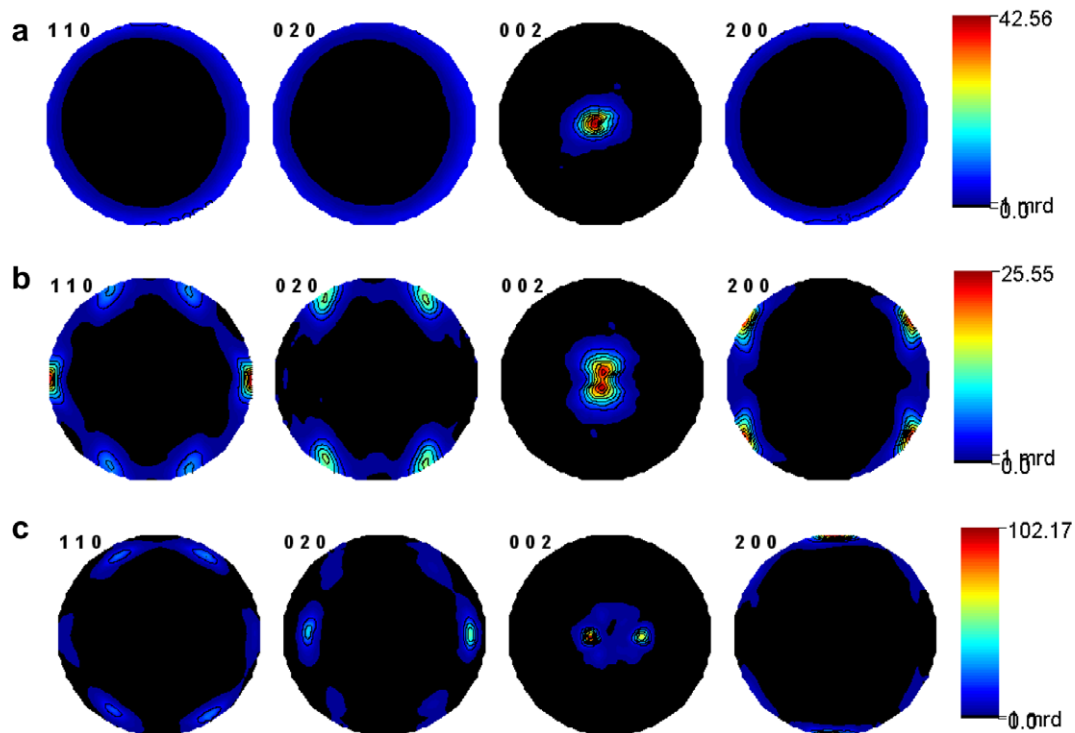


Fig. 6. {110}, {020}, {002} and {200} recalculated normalised pole figures of the (a) outer (b) intermediate and (c) inner layers. Linear density scale, equal area projections.

main $\langle 110 \rangle$ directions along **M**, quite as in *P. tabularis*, while *Scutus antipodes* aligns the main $\langle 110 \rangle$ with **G**.

The inner comarginal crossed lamellar (ICCL) layer of *C. lampas lampas* (Fig. 6c) exhibits the strongest texture (Table 1). With a texture index around 721 mrd^2 and a maximum of the {002} pole figure at 102 mrd , this texture is among the strongest observed to date in shells. This is coherent with the largest organisation of the lamellae observed using SEM. The strongest 002 poles are located at 20° from **N** and two major *c*-axis components are visible in the (**M,N**) plane, forming an opening angle of 40° . However, four other smaller 002 poles are visible. These are due to double twinning in this layer, as visible on the {020} pole figure which shows six 020 contributions. In this layer the main {200} contribution

aligns with **G**, and the double twinning percentage is of 80%. From the species of which the texture of the ICCL layer was already studied, *Cypraea testudinaria* is the only one showing a close texture pattern with *C. lampas*, though its *a*-axis distributions are not twinned-like (Chateigner et al., 1996).

3.3. Texture and SEM microstructure relationship

It is interesting to notice once more that SEM images could have induced incorrect crystal orientation definitions, and even misinterpretations of the layer types if not carefully examined. Indeed for the outer layer, at a first glance, Fig. 2a would indicate a comarginal layer, while texture analysis clearly demonstrates the crossed

lamellae are distributed around **N** at a larger scale. This layer is then neither radial nor comarginal, but the orientations of lamellae vary from a location to the other at a few hundred micrometres scale. Furthermore, the {002} pole figure of this layer (Fig. 6a) shows a unique orientation component, demonstrating that the plane of the second-order lamellae and their elongated axis are not corresponding to low indices crystallographic planes and axes, respectively. The closest crystal planes that would fit the orientation of the observed SEM second-order lamellae are {111}.

Concerning the intermediate and inner layers, the twofold *c*-axis distribution (Fig. 5b and c, respectively) gives rise to another degree of freedom for the assignment of specific crystal planes to the SEM images. The normals to the second-order lamellae are not aligned with the {002} poles, and twinning adds to the complexity. The distributions of the {002} pole components could correspond to the distribution of second-order lamellae orientations (visible in Fig. 4b, bottom centre), but their planes are not {002}. The second-order lamellae are again oriented with their normal at around 40–50° from **N** for both layers, and as was the case in the outer layer. It then comes that whatever the crystalline orientation differences observed by X-ray diffraction on the three layers, their SEM images look similar in terms of platelets orientations from **N**. SEM observations are providing neat definitions of how the microstructure looks at a 10 nm to several 100 μm, but are not able to visualise twinned patterns, split *c*-axis or other ordering patterns at a larger scale, even on a qualitative point of view. For instance, radial and comarginal CL layers as defined from SEM can correspond to very different orientations of the crystal axes in the layers. In the literature, RCL layers are corresponding to different *a*-axis orientation patterns, which might lead to confusion when dealing with biomineralisation.

3.4. Texture and phylogeny

Chateigner et al. (1999) introduced a texture terminology for mollusc shells which groups in one term all the textural information. From the outer to the inner layer, the texture of *C. lampas lampas* can then be summarised by: $\langle \perp | \text{OCL} | \rangle$, $\langle \vee, 20 | \text{RCL} | \times_{100}^{(110),90} \rangle$, $\langle \vee, 40 | \text{ICCL} | *_{80}^a \rangle$. It is clearly not the purpose of this work to elaborate on the taxonomic location of *C. lampas* in the gastropod phylogeny based on texture observations, nor to include textural characters into parcimonial approaches or calculations. But we wanted to examine if the textural characterisation of this species at least fits with the actually developed classifications.

Among all the aragonitic layers of gastropods for which a texture term has been described in the literature, which represents a set of around 50 layers only, the layer species that exhibit split *c*-axis are:

- The inner irregular complex crossed lamellar layer (IICCL) of *Fisurella oriens*: $\langle \vee, 20 | \text{IICCL} | *_{83}^{(110)} \rangle$.
- The ICCL and RCL layers of *Cypraea testudinaria*: $\langle \vee, 15 | \text{ICCL} | *_{80}^a \rangle$ and $\langle \vee, 25 | \text{RCL} | \times_{100}^{(110),75} \rangle$, respectively.
- The IRCL layer of *Patella tabularis*: $\langle \vee, 25 | \text{IRCL} | \times_{100}^{(110),100} \rangle$
- The operculum inside (OI) layer (unpublished result) of *Nerita scabricosta*: $\langle \vee, 45 | \text{OI} | \rangle$.

In the case of *F. oriens*, the opening angle of the *c*-axis distribution is smaller than for *C. lampas*, the crossed lamellar layer is irregular and the {110} directions (versus *a*-axis in *C. lampas*) are aligned with **G**. This tends to put some phylogenetic distance between the two species. The split *c*-axis are only found in the OI layer of *N. scabricosta*, which furthermore exhibits a calcitic outer layer, and an inner fibre texture. The IRCL of *P. tabularis* is very close to the RCL of *C. lampas* from a textural term point of view,

but this is most probably the only close resemblance the two gastropods could reveal! Finally, the simple comparison of the texture terms of these four species with the corresponding layers of *C. lampas* is coherent with the relative proximity of this latter with *Cypraea testudinaria*. *C. testudinaria* shows other layers (Chateigner et al., 2000) which all exhibit texture terms different from the remaining OCL of *C. lampas*, and it then becomes also coherent to classify the two species in distinct families, as generally admitted (Ponder and Lindberg, 1997; Bouchet and Rocroi, 2005).

3.5. Cell parameters and distortion of aragonitic shell

One of the issues of the combined analysis is the refinement of the structure, in particular the cell parameters of aragonite, together with the texture. Using X-ray diffraction it was not expected any sensitivity on the C and O atomic positions in the CaCO₃ structure because of the larger contrast between electron densities of these atoms and Ca. The key point of this study is that combined analysis is able to carry out unit-cell refinement on real samples, without needs of powderising the specimen even if they exhibit strong and complex textures. Although we used a laboratory equipment [Ricote et al., 2004], this latter is resolved enough to provide reasonably precise cell parameters and then potentially allows the observation of unit-cell distortions due to organic molecules. In order to verify our poor sensitivity on light atom positions, we started to release one by one atomic positions, for the Ca, C and then O atoms successively. Unexpectedly we discovered that the combined methodology gave access with reasonable standard deviations to all the positions (see below) within comprehensive values. We attribute this to the fact of working on strongly textured samples (closer to single crystals than to powders), for which angular information between atomic bounds is stressed by their coherence in orientations via the OD.

Refined cell parameters are summarised in Table 1 for the three layers. We observe deviations from the usual non-biogenic aragonite for all cell parameters and layers, *a*, *b* and *c* being larger in the biocomposite layers of *C. lampas lampas* except for *b* in the inner layer. The increases correspond to relative parameter distortions ranging from 0% for *b* in the ICCL layer to 0.53% for *b* in the Outer CL layer. As an evidence the cell distortions are anisotropic and the relative unit-cell volume increase differs in the three layers, being less pronounced in the intermediate layer. The *b* and *c* cell parameters show an opposite evolution from the OCL to the ICCL layers, while *a* oscillates and takes its lowest value for the intermediate RCL layer. Similar cell distortions were already observed in biogenic aragonite layers using high resolution synchrotron instruments (Pokroy et al., 2006), on powderised shells of various species from the Mollusca. The authors observed much lower cell distortions, also anisotropic, around three times less than our maximum observation. Using specific sample preparation, the authors could remove the intercrystalline organics hereby attributing the cell distortions to the intracrystalline interactions between organic macromolecules and mineral aragonite. Pokroy et al. (2007) were able remarkably to associate these distortions to a variation of the aplanarity of the CO₃ groups in the studied species, using atomic position refinement from neutron powder diffraction. In our case, we worked on real layers, neither powderised, nor bleached to remove intercrystalline macromolecules. In that sense, a possible intercrystalline effect remains visible as a cell distortion, cumulated to the intracrystalline influence. Intercrystalline macromolecules have been associated to the selection of calcium carbonate polymorphism (Falini et al., 1996) and to the development of textures in mollusc shells, a process involving a spatial organisation of macromolecular cells in which the mineral phase nucleates and orients. However, as soon as intercrystalline organic matter is able to constrain mineral textures, one cannot exclude a

possible effect on the crystallite cells. Such an effect would explain why we observe larger cell distortions than previously observed by Pokroy and collaborators. But the powderisation of the layers could also bias the cell distortion analysis. On one hand, strains imposed by intercrystalline organics, or by layer stacking, could be partially released during this step or other preparation of the specimen. This would make difficult the comparison of our results with the ones of previous authors. On the other hand, the destruction of the biocomposite texture could make the observation of anisotropy more difficult, as was already shown for crystallite shape analysis (Morales et al., 2005).

The textured layers analysed in this work all show anisotropies of the cell distortion that are different from the ones coming from the sole intracrystalline molecular influence. In particular, we do not observe negative relative distortions on real layers, and the most distorted cell parameter is not the same in all layers, as a sign of the crystalline orientation influence on the distortion. In such a way, all cell parameters are elongated, but this does not correspond to the establishment of residual stresses occasioned by macromolecule intercalations, since we did not observe peak shifts when inclining the sample under X-rays (Fig. 5). Pokroy et al. (2006) demonstrated a quite constant intracrystalline molecules influence for several sea-water gastropod, bivalve and cephalopod species. Among the animal they studied, the phylogenetically closest to *Charonia* was *Strombus decorus persicus*, which also possesses a crossed lamellar layer. Among all the species they measured, *Haliotis lamellosa* has an a priori known texture of its inner columnar nacre layer (its texture should resemble the $\langle 001 \rangle$ fibre ones of *H. cracherodi*, *H. haliotis* and *H. rufescens* we already measured). The textures and microstructures of *Haliotis* species and *Charonia* are very different in character and strength. It then becomes interesting to notice that if intracrystalline macromolecules can create similar distortion levels in such distant species, they have probably a very weak role in the development of the microstructures and textures, these latter being in turn controlled by intercrystalline entities.

The refined atomic positions for the three layers of *Charonia*, the non-biogenic sample taken as reference, and the *Strombus* results from Pokroy et al. (2007) are listed in Table 2. One can observe the low standard deviations obtained even for C and O atoms. We were not sensitive to the thermal vibrations and did not release these parameters during the refinements. As Pokroy and collaborators mentioned, one indicator of the structural modifications within the aragonite structure is the distance $\Delta Z_{C-O1} = (z_C - z_{O1})c$

between the carbon atoms and the oxygen planes, a distance that goes to 0 for calcite and reveals the aplanarity of the CO_3 groups. We observe that this distance in the three *Charonia* layers increases from the outer to the inner layer, reaching 0.1 Å in this latter. Interestingly, the average value of ΔZ_{C-O1} over the three layers is 0.05 Å, quite the value of the non-biogenic sample. Hence, powderising a sample like *Charonia*, if all the intercrystalline effects not removed, would have given a value close to a non-biogenic specimen, hereby masking any organic macromolecule effect. Of course such a comparison stands only for *Charonia* as each layer type (nacre, prismatic, etc.) can provide with different ΔZ_{C-O1} values giving rise to different averages. In this species, the aplanarity of the carbonate groups is reinforced in the inner layer (quite twice the one of the non-biogenic reference), then diminishes inside the intermediate layer, to practically cancel in the outer layer. On many mainly aragonitic mollusc species a calcitic layer is found on the outer shell, and this aplanarity decrease towards the outer layer in *Charonia* tends to 0 as for calcite. This newly observed behaviour is for us another expression (together with textural strength decrease) of the control loss from the macromolecules on aragonite stabilisation farther from the animal.

3.6. Colours to crystalline textures

Pigments at the origin of colours at the surface of many mollusc shells have been identified either as carotenoids (Koizumi and Nonaka, 1970, Dele-Dubois and Merlin, 1981), carbohydrates (Akamatsu et al., 1977), porphyrins (Jones and Silver, 1979), polyenes (Hedegaard et al., 2006). Looking at the organisation of the crystallites in the outer layers of gastropods and at their colour patterns on the shell surface might implicate a relationship between the two. For instance, the strong orientation of *Helix aspersa* and its inclined brown bands have been shown to follow the same $\langle 020 \rangle$ directions. *C. lampas lampas* brownish bands and spots are aligned with the growing direction. However, texture analysis indicates a fibre texture, meaning that in the plane of the shell surface there is no systematic crystalline direction aligned with **G**. This clearly prevents any relationship between the two crystalline and colour textures in this species. For gastropod shells with determined textures (Chateigner et al., 2000), many exhibit colour textures on their outer layer whereas crystalline textures are fibres, e.g., *Conus leopardus*, *Cyclophorus woodianus*, *Tectus niloticus*, *Entemnotrochus adansonianus*, etc., all belonging to the Prosobranchia.

Table 2
Cell parameters, refined atomic positions and ΔZ values for *Charonia* layers, our non-biogenic reference and the *Strombus* species of Pokroy et al. (2007)

	Geological reference	<i>Charonia lampas</i> OCL	<i>Charonia lampas</i> RCL	<i>Charonia lampas</i> ICCL	<i>Strombus decorus</i>
<i>a</i> (Å)	4.9623(3)	4.98563(7)	4.97538(4)	4.9813(1)	4.9694(3)
<i>b</i> (Å)	7.968(1)	8.0103(1)	7.98848(8)	7.9679(1)	7.9591(4)
<i>c</i> (Å)	5.7439(3)	5.74626(3)	5.74961(2)	5.76261(5)	5.7528(1)
Ca					
<i>y</i>	0.415	0.41418(5)	0.414071(4)	0.41276(9)	0.4135(7)
<i>z</i>	0.7597	0.75939(3)	0.76057(2)	0.75818(8)	0.7601(8)
C					
<i>y</i>	0.7622	0.7628(2)	0.76341(2)	0.7356(4)	0.7607(4)
<i>z</i>	−0.086	−0.0920(1)	−0.08702(9)	−0.0833(2)	−0.0851(7)
O1					
<i>y</i>	0.9225	0.9115(2)	0.9238(1)	0.8957(3)	0.9228(4)
<i>z</i>	−0.096	−0.09205(8)	−0.09456(6)	−0.1018(2)	−0.0905(9)
O2					
<i>x</i>	0.4736	0.4768(1)	0.4754(1)	0.4864(3)	0.4763(6)
<i>y</i>	0.681	0.6826(1)	0.68332(9)	0.6834(2)	0.6833(3)
<i>z</i>	−0.086	−0.08368(6)	−0.08473(5)	−0.0926(1)	−0.0863(7)
ΔZ_{C-O1} (Å)	0.05744	0.00029	0.04335	0.1066	0.031

Parentheses indicate standard deviations on the last digit.

In this subclass there is then probably no determined relationship used by the molecules in the periostracum between colour and crystal textures. However, up to now, all the strong crystallographic textures observed in the Pulmonata indicate that the (020) direction aligns with the coloured bands of the outer layer. We only found in the literature four species of this order for which the crystalline texture was determined (*H. aspersa*, *H. pomatia*, *Euglandina* sp. and *Helminthoglypta nickliniana anachoreta*) and our observation cannot be matter for generalisation, but rather if links exist between macromolecules that induce crystal orientations and the ones responsible for coloured bands, perhaps these species can serve their determination.

3.7. Elastic anisotropic behaviour of the mineral phase

Preferred orientations condition mechanical properties of aggregates, in particular when the constituting crystals possess strong anisotropy of their elastic stiffness constants. We then wanted to estimate the elastic mechanical behaviour of the different layers of *Charonia*, as provided by the mineral part. For single phase materials, the calculation of the OD-weighted average of the single crystal stiffness tensor provides the specimen macroscopic tensor, under the hypothesis of regular grain boundary behaviours (Kocks et al., 1998). In this aim and conditions, the geometric mean approach has been shown to be as reliable as more sophisticated techniques like self-consistent calculations (Matthies and Humbert, 1995). In the case of shell layers, with their biocomposite nature, we are far from single phase compounds, and crystallite interactions are mainly present at the boundaries. But to the authors' knowledge it does not exist at the present time some methodology to take account of all the complex characteristics of this composite. With this respect, we only intend in the following to illustrate what the mineral part of the shell brings as an elastic behaviour to the ultrastructure.

Table 3 shows the macroscopic elastic stiffness tensors calculated using the geometric mean approach and the orientation distribution of crystallites, for the mineral part of the three layers of *Charonia*. For aragonite there are nine independent values for c_{ij} , c_{ii} ($i = 1-6$), c_{12} , c_{13} and c_{23} , which we took from the literature for

the single crystal values. In the frame of this calculation, axes 1, 2 and 3 for i and j indices are the **M**, **G** and **N** directions, respectively. One can remark several orientation effects on the macroscopic constants of the layers. First of all, the c_{33} constant remains unchanged around 85 GPa whatever the layer, and keeps quite the value of the single crystal. This is provided by the strong c -axis orientation with **N** on average in the three layers. For the ICCL and RCL layers, one can remark that the c -axis splitting on average induces a slightly lower c_{33} than in the OCL layer. This relatively large value ensures rigidity along the normal to the shell. In the inner layer, the c_{11} and c_{22} magnitudes have been reversed compared to the single crystal, c_{22} being larger in the ICCL layer. This comes from the strong alignment of the a -axis along **G** (Fig. 6c) in this layer. In the intermediate RCL layer the phenomenon is reversed, with a larger c_{11} as in the single crystal, giving rise to a stronger rigidity along **M** for this layer, with, however, less difference between c_{11} and c_{22} . The textures of the ICCL and RCL layers then accommodate a strong rigidity alternatively along **G** and **M**, making a stack which beneficiates of a strong c_{11} coefficient along the two main directions in the shell plane. Interestingly, the $c_{11} - c_{22}$ quantity decreases from the inner to the outer layers, revealing the progressive through thickness anisotropy decrease. In the (001) fibre texture of the OCL layer, this difference is quite 0, indicating and equivalent response of the mineral to compression along **G** and **M**, and other in-plane directions. All the off-diagonal c_{ij} coefficients are homogenised in the layers, being much less anisotropic than in the single crystal. This is a way to moderate transverse deformations in the shell as an overall on the three layers. The shear coefficients c_{44} , c_{55} and c_{66} also obey a balancing tendency from one layer to the other, and in particular c_{44} and c_{55} . Again here the overall shell composed of the alternate orientations of the layers possesses maximum shear coefficients along all the directions of the whole shell.

To summarise, from an elastic anisotropic theory point of view, the stacking of the three crossed lamellar layers with strong textures behave, only looking at their mineral parts, in an optimised manner relative to compression and shear. The alternating shapes of the orientations provided by the animal operate the largest stiffness coefficients in all directions of the whole shell for these two types of sollicitation.

Table 3

Macroscopic elastic stiffness c_{ij} tensors (in GPa) for a single crystal of aragonite (Voigt, 1928), and the mineral part of the three layers of *Charonia* as calculated from the OD using the geometric mean

Single crystal	160	37.3 87.2	1.7 15.7 84.8	41.2	25.6	42.7
ICCL layer	96.5	31.6 139	13.7 9.5 87.8	29.8	36.6	40.2
RCL	130.1	32.6 103.3	10.3 14.1 84.5	36.3	31.1	40.5
OCL	111.1	32.9 119	13.2 11.8 84.8	32.8	34.6	40.9

4. Conclusion

SEM and X-ray diffraction characterisation have been used to investigate a *C. lampas lampas* shell. SEM investigations reveal that this species is composed of three distinct, inner comarginal crossed lamellar, intermediate radial crossed lamellar and outer crossed lamellar layers. Using the X-ray diffraction combined analysis approach we determined quantitatively the textures of the three layers, their respective aragonite unit-cell distortions, and the macroscopic elastic tensor of their mineral parts. Textures of the three layers are very strong, with an overall decrease of the texture strength from the inner layer outward. While the inner and intermediate layers show regular texture patterns for crossed lamellae, with split c -axis component around the shell normal and double and single twinning patterns for their a -axis, respectively, the outer crossed lamellae appear randomly distributed around c in the outer layer, at the few mm^2 scale, giving rise to a fibre texture. The texture information is coherent with the usually admitted gastropods phylogeny for this taxon. An anisotropic unit-cell distortion is quantified for the three layers without necessity of powderising them. These distortions are attributed to the combined effects of inter- and intracrystalline macromolecules, by comparison with other authors works. No colour to crystalline texture relationship could be detected in this species. Finally the sim-

ulation of the macroscopic elastic tensors of the mineral part of the layers could be possible using texture data. This simulation shows that the strong orientations present in the successive layers render maximum benefits to the shell in terms of rigidity and shear resistance.

References

- Akamatsu, S., Komatsu, H., Koizumi, C., Nonaka, J., 1977. A comparison of sugar components of yellow and white pearls. *Nippon Suisan Gakkaishi* (Bulletin of the Japanese Society of Scientific Fisheries) 43, 773–777.
- Bazylnski, D.A., 1996. Controlled biomineralization of magnetic minerals by magnetotactic bacteria. *Chemical Geology* 32, 191–198.
- Beu, A.G., 1985. A classification and catalogue of living world Ranellidae (=Cymatiidae) and Bursidae. *Conchologists of America Bulletin* 13 (4), 55–66.
- Beu, A.G., 1987. Taxonomy of gastropods of the families Ranellidae (=Cymatiidae) and Bursidae. Part 1. Adoption of Ranellidae, and review of Linatella Gray, 1857. *New Zealand Journal of Zoology* 13, 241–266.
- Bouchet, P., Rocroi, J.-P., 2005. Classification and nomenclator of gastropod families. *Malacologia* 47 (1–2), 1–397.
- Cariolou, M.A., Morse, D., 1988. Purification and characterization of calcium-binding conchiolin shell peptides from the mollusc *Haliotis rufescens*, as a function of development. *Journal of Comparative Physiology B* 157, 717–729.
- Carter, J.G., Clark II, G.R., 1985. Classical and phylogenetic significance of molluscan shell microstructure. In: Bottjer, D.J., Hickman, C.S., Ward, P.D., Broadhead, T.W. (Eds.), *Molluscs, Notes for a Short Course*. University of Tennessee, Department of Geological Sciences Studies in Geology, pp. 50–71.
- Chateigner, D. (Ed.), 2004. Combined Analysis: Structure–Texture–Microstructure–Phase–Stresses–Reflectivity Analysis by X-ray and Neutron Scattering, 150p. Available form: <<http://www.ecole.ensicaen.fr/~chateign/texture/combined.pdf>>.
- Chateigner, D., 2005. Reliability criteria in quantitative texture analysis with experimental and simulated orientation distributions. *Journal of Applied Crystallography* 38, 603–611.
- Chateigner, D., Hedegaard, C., Wenk, H.-R., 1996. Texture analysis of a gastropod shell: *Cypraea testudinaria*. In: Liang, Z., Zuo, L., Chu, Y. (Eds.), *Textures of Materials*, vol. 2. Int. Academic Publishers, pp. 1221–1226.
- Chateigner, D., Hedegaard, C., Wenk, H.-R., 1999. Quantitative characterisation of mollusc shell textures. In: Szpunar, J.A. (Ed.), *Textures of Materials*, vol. 2. NRC Research Press, pp. 1495–1500.
- Chateigner, D., Hedegaard, C., Wenk, H.-R., 2000. Mollusc shell microstructures and crystallographic textures. *Journal of Structural Geology* 22 (11–12), 1723–1735.
- Chen, B., Peng, X., Wang, J., Sun, S., in press. Investigation of interlaced microstructure of aragonite sheets of *Chamidae* shell. *Comparative Material Science*.
- Currey, J.D., 1977. Mechanical properties of mother of pearl in tension. *Proceedings of the Royal Society of London B: Biological Sciences* 196, 443–463.
- Dele-Dubois, M.L., Merlin, J.C., 1981. Etude par spectroscopie Raman de la pigmentation du squelette calcaire du corail. *Revue de Gemmologie* 68, 10–13.
- Falini, G., Albeck, S., Weiner, S., Addadi, L., 1996. Control of aragonite or calcite polymorphism by mollusk shell macromolecules. *Science* 271, 67–69.
- Hare, P.E., Abelson, P.H., 1965. Amino Acid Composition of Some Calcified Proteins. *Year Book-Carnegie Inst., Washington*, vol. 65, pp. 223–232.
- Hedegaard, C., Bardeau, J.-F., Chateigner, D., 2006. Molluscan shell pigments: an in situ resonance Raman study. *Journal of Molluscan Studies Advance Access* 72, 157–162.
- Kamat, S., Su, X., Ballarini, R., Heuer, A.H., 2000. Structural basis for the fracture toughness of the shell of the conch *Strombus gigas*. *Nature* 405, 1036–1040.
- Kocks, F., Tomé, C., Wenk, H.-R. (Eds.), 1998. *Texture and Anisotropy*. Cambridge University Press, Cambridge.
- Koizumi, C., Nonaka, J., 1970. Yellow pigments of pearl I. Carotenoid pigment in yellow nacre. *Nippon Suisan Gakkaishi* (Bulletin of the Japanese Society of Scientific Fisheries) 36, 1054–1058.
- Lowenstam, H.A., 1967. Lepidocrocite, an apatite mineral, and magnetite in teeth of chitons (Polyplacophora). *Science* 156, 1373–1375.
- Lutterotti, L., Matthies, S., Wenk, H.-R., 1999. MAUD (Material Analysis Using Diffraction): A User Friendly Java Program for Rietveld Texture Analysis and More. National Research Council of Canada, Ottawa, 1999, pp. 1599–1604.
- Lutterotti, L., Chateigner, D., Ferrari, S., Ricote, J., 2004. Texture, residual stress and structural analysis of thin films using a combined X-ray analysis. *Thin Solid Films* 450, 34–41.
- Jackson, A.P., Vincent, J.F.V., Turner, R.M., 1990. Comparison of nacre with other ceramic composites. *Journal of Material Sciences* 25, 3173–3178.
- Jones, P., Silver, J., 1979. Red and blue-green bile pigments in the shell of *Astraea tuber* (Mollusca: Archaeogastropoda). *Comparative Biochemistry and Physiology Series B* 63, 185–188.
- Morales, M., Leconte, Y., Rizk, R., Chateigner, D., 2005. Structural and microstructural characterization of nanocrystalline silicon thin films obtained by radio-frequency magnetron sputtering. *Journal of Applied Physics* 97, 034307.
- Matthies, S., Humbert, M., 1995. On the principle of a geometric mean of even-rank symmetric tensors for textured polycrystals. *Journal of Applied Crystallography* 28, 254–266.
- Murphy, W.L., Mooney, D.J., 2002. Bioinspired growth of crystalline carbonate apatite on biodegradable polymer substrata. *Journal of the American Chemical Society* 124 (9), 1910–1917.
- Ouhenia, S., Chateigner, D., Belkhir, M.A., Guilmeau, E., Krauss, C., 2008. Synthesis of calcium carbonate polymorphs in the presence of polyacrylic acid. *Journal of Crystal Growth* 310 (11), 2832–2841.
- Ponder, W.F., Lindberg, D.L., 1997. Towards a phylogeny of gastropod molluscs: an analysis using morphological data. *Zoological Journal of the Linnean Society* 119 (2), 83–265.
- Pokroy, B., Quintana, J.P., Caspi, E.N., Berner, A., Zolotoyabko, E., 2004. Anisotropic lattice distortions in biogenic aragonite. *Nature Materials* 3, 900–902.
- Pokroy, B., Fitch, A.N., Lee, P.L., Quintana, J.P., Caspi, E.N., Zolotoyabko, E., 2006. Anisotropic lattice distortions in mollusc-made aragonite: a widespread phenomenon. *Journal of Structural Biology* 153, 145–150.
- Pokroy, B., Fieramosca, J.S., Von Dreele, R.B., Fitch, A.N., Caspi, E.N., Zolotoyabko, E., 2007. Atomic structure of biogenic aragonite. *Chemistry of Materials* 19, 3244–3251.
- Ricote, J., Chateigner, D., Morales, M., Calzada, M.L., Wiemer, C., 2004. Application of the X-ray combined analysis to the study of lead titanate based ferroelectric thin films. *Thin Solid Films* 450, 128–133.
- Sakaguchi, T., Burgess, J.G., Matsunaga, I., 1993. Magnetite formation by a sulphate-reducing bacterium. *Nature* 365, 47–49.
- Smith, B.L., Schaffer, T.E., Viani, M., Thompson, J.B., Frederick, N.A., Kind, J., Belcher, A., Stucky, G.D., Morse, D.E., Hansman, P.K., 1999. Molecular mechanistic origin of the toughness of natural adhesives, fibres and composites. *Nature* 399, 761–763.
- Sugawara, A., Kato, T., 2000. Aragonite CaCO₃ thin-film formation by cooperation of Mg²⁺ and organic polymer matrices. *Chemical Communications* 6, 487–488.
- Voigt, W., 1928. *Lehrbuch der Kristallphysik*. Leipzig, Teubner.